

An ultrastrongly coupled single THz meta-atom

Shima Rajabali^{1,*}, Sergej Markmann¹, Elsa Jöchl¹, Mattias Beck¹, Christian A. Lehner², Werner Wegscheider², Jérôme Faist¹, Giacomo Scalari^{1,*}

¹*Institute of Quantum Electronics, ETH Zürich, 8093 Zürich, Switzerland*

²*Laboratory for solid state physics, ETH Zürich, 8093 Zürich, Switzerland*

Free-space coupling to strongly subwavelength individual optical elements is a central theme in quantum optics, as it allows to control and manipulate the properties of quantum systems. In this work, we show that by combining an asymmetric immersion lens setup and complementary design of metasurfaces we are able to perform THz time domain spectroscopy of an individual, strongly subwavelength ($\frac{d}{\lambda_0} = 1/20$) meta-atom. We unravel the linewidth dependence of planar metamaterials as a function of the meta-atom number indicating quenching of the Dicke superradiance. On these grounds, we investigate ultrastrongly coupled Landau polaritons at the single resonator level, measuring a normalized coupling ratio of $\frac{\Omega}{\omega} = 0.60$ resulting from coupling of the fundamental mode to a few thousand electrons. Similar measurements on a low loss, less doped two dimensional electron gas yield a coupling ratio $\frac{\Omega}{\omega} = 0.33$ with a cooperativity $C = \frac{4g^2}{\kappa\gamma} = 94$. Interestingly, the coupling strength of a coupled single resonator is the same as of a coupled array. Our findings pave the way towards the control of light-matter interaction in the ultrastrong coupling regime at the single electron/single resonator level. The proposed technique is way more general and can be useful to characterize

the complex conductivity of micron-sized samples in the THz and sub-THz domain.

Extreme electronic and photonic confinement has recently allowed a number of groundbreaking advances in several fields, from fundamental studies ¹ to applications ^{2,3}. Particularly interesting is the possibility to manipulate *on-chip* the light-matter coupling achieving new quasi-particles called cavity polaritons ⁴ that profoundly modify the electro-optical properties of the constituent elements.

Cavity polaritons rely on enhanced vacuum field fluctuations \mathcal{E}_0 to reach large values of the vacuum Rabi frequency $\Omega_R \propto \mathcal{E}_0$ quantifying large values of coupling ⁵. The dependence from the inverse of the cavity volume $\mathcal{E}_0 \propto 1/\sqrt{V}$ led to the development of strongly subwavelength structures to reach the strongest couplings to-date ^{6,7}. Metallic-based cavities have been used in the mid-infrared (Mid-IR)⁸ and terahertz (THz)⁹ regions of the electromagnetic spectrum for strong coupling experiments. Due to their subwavelength nature, the experiments have been carried out on multiple cavities (100 – 1000 or more) in order to enhance the signal-to-noise ratio (SNR). Since the frequency components excited for subwavelength features cannot propagate in the far-field, only recently near-field techniques proved to be successful in probing single resonator-based strongly coupled systems at Mid-IR frequencies at room temperature ^{10,11}. In the field of ultra-strong coupling, the development of the Landau polariton platform¹² has led to very fascinating results, including studies of non-linear phenomena ¹³, the reaching of high cooperativity ¹⁴ and the study of magnetotransport ¹⁵ in ultrastrongly coupled Hall systems ¹⁶. In this approach, extremely subwavelength planar split-ring resonators have been used in combination with one-dimensionally

confined semiconductor heterostructures to achieve normalized coupling values $\frac{\Omega}{\varepsilon} > 1.4$ (Ref ¹⁷).

The light-matter interaction strength in most of the solid-state-based cavity quantum electrodynamics (QED) systems scales with \sqrt{N} with N electron number due to the collective (Dicke) enhancement of the interaction strength¹⁸. In Landau polaritons, when employing metasurface cavities, the number of coupled electrons is shared among several hundreds of identical cavities. In the last few years, there has been a growing interest in studying ultrastrong light-matter coupled systems towards the limit of few electrons coupled to a single cavity ^{19–21} to study the fermionic Rabi model for the coupled systems rather than the bosonic Hopfield description where both material excitation and the electromagnetic field are described as boson fields. Moreover, such systems can be building blocks for performing quantum information tasks. In this perspective a reduction in the number of coupled carriers towards the low limit of a few and ultimately a single coupled element constitutes a great challenge both in terms of measurement sensitivity ^{1,22} and optical cavity design.

The possibility and the limits on the interaction of free propagating far-field optical beams from individual elements (molecules, atoms, quantum dots etc...) have been investigated both theoretically ^{23,24} and experimentally ^{25,26}, mainly at visible or infrared frequencies. In our case the individual element is not a quantum object but rather a single-subwavelength metallic planar resonator, operating at millimeter wavelengths, lying in-between free space propagating beams and guided microwaves. The single resonator spectroscopy at sub-THz/THz spectrum is performed by implementing a simple and practical asymmetric Silicon immersion lens (aSIL) configuration. We

also demonstrate the linear dependence of the cold cavity linewidth of a 2D array of the meta-surface on the number of resonators in the array when the illuminated area with resonators becomes comparable or smaller than the wavelength. This observation is an indication of quenching the superradiance decay. Moreover, the Landau polaritons in a coupled single-subwavelength resonator are resolved on two different semiconductor heterostructures, and high normalized coupling strength up to 60% and high cooperativities up to $C = 94$ are achieved.

Measurements and results

Single resonator detection and superradiance Free-space probing of a sample containing a few/single subwavelength resonators is difficult as it is intrinsically inefficient in exciting the right electromagnetic modes and generally features a very low signal-to-noise ratio. We thus developed a strategy based on the employment of the complementary metamaterial approach combined with an aSIL configuration to optimize the matching of a free space propagating beam to a single element of a complementary metasurface. The conventional THz-time domain spectroscopy (TDS) setup has a pair of off-axis parabolic mirrors first to collimate and then focus the incident THz beam from the photo-conductive switch²⁷ on the sample. The transmitted signal from the sample will be then collected, collimated, and then focused on the ZnTe crystal through another pair of off-axis parabolic mirrors (Fig. 1a). The detection is performed using an electro-optic detection scheme²⁸. The beam, that we can assume has a Gaussian profile, in this setup has a spot size of around $3mm$ at the sample's location. In order to correctly match the incoming THz beam to the single complementary meta-atom, we designed a back-to-back lens system inspired by some pre-

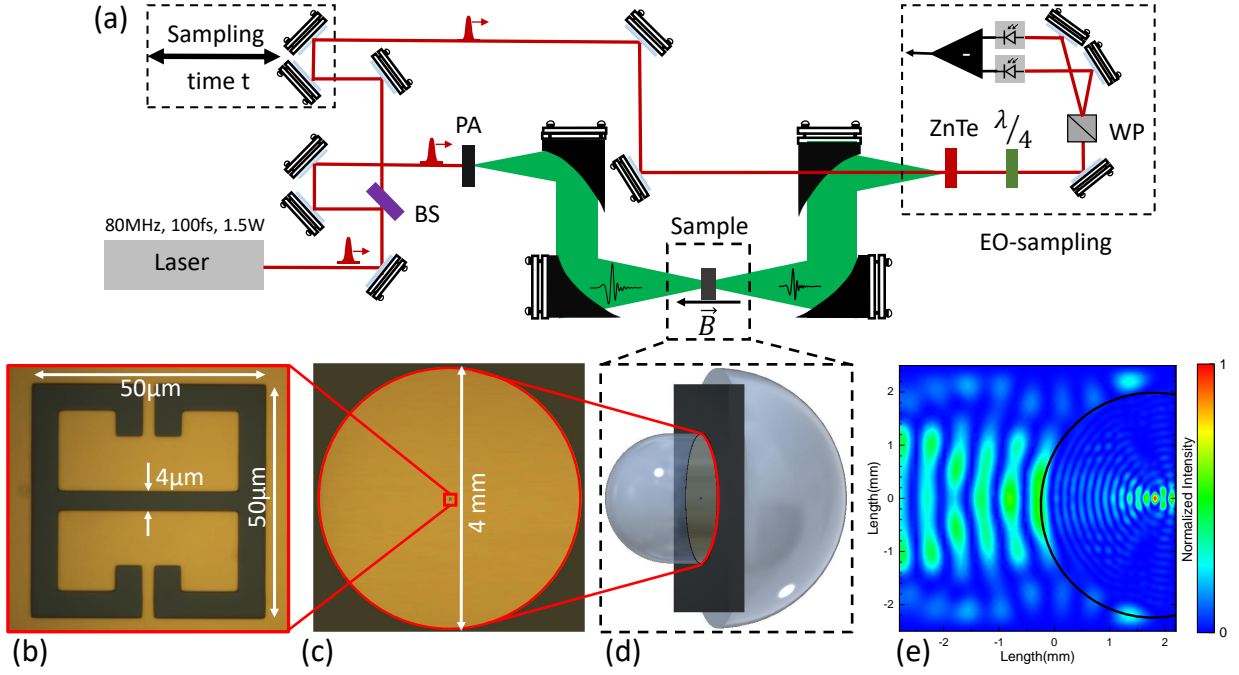


Figure 1: **Schematic of the TDS setup with the aSIL configuration** (a) The schematic sketch of the THz-TDS used for the transmission experiments. (b) The optical image of the single resonator including the periodicity and gap size. (c) The optical image of the whole sample metallized with a circular boundary of diameter 4mm for the alignment of the front lens. (d) The magnified schematic of the aSIL configuration. (e) The COMSOL simulation result of the focused THz beam at the interface between the front lens and the resonator field.

vious studies on single quantum dots at visible wavelengths²⁶ (Fig. 1d). Being very akin to a $4f$ arrangement, a similar setup has been recently proposed also as a THz spatial filter²⁹. A set of ray optics simulations in COMSOL Multiphysics is done to find the correct lens dimensions and adjust the input and output numerical aperture of the system such that it is compatible with the existing THz-TDS setup. A final design consists of a front hyperhemispherical Silicon (Si) lens of diameter $4mm$ that focuses the incident beam to a spot size of $\sim 500\mu m$ at the surface of the sample (Fig. 1e), where the metamaterial resonators are located. The back hemispherical Si lens of diameter $8mm$ collects the transmitted beam from the sample and sends it through the off-axis parabolic mirrors to the detector. To optimize the dimensions for the back lens, we run a parametric sweep on the back lens diameter in the COMSOL simulation. The goal was to match the output numerical aperture of the lens system with the numerical aperture $f\#3.85$ of the off-axis parabolic mirror according to the chosen thickness and material for the substrate at the operating frequency ($f = 300GHz$). In our case, we used a $500\mu m$ thick semi-insulating gallium arsenide (GaAs) slab that corresponds to the average thickness of the substrates used for the epitaxial growth of the samples. The presence of the substrate where the sample is deposited also makes the back lens effectively an hyperhemispherical one. The significant advantage of this asymmetric design compared to the previous symmetric designs^{26,29} is that there is no need to sandwich the target surface (in our case, the metamaterial metallic thin film) between two semiconducting substrates to have the surface at the focus point of the confocal system. The asymmetry of the lenses accounts for the sample substrate thickness as an active part of the optics. The sample itself is located on top of the substrate and has a very small thickness compared to the wavelength. The planar com-

plementary metasurface and the underlying quantum well (QW) sum up to less than $1\mu m$ in the propagation direction of the THz beam. Thus the back lens with a larger diameter compensates for the substrate thickness and collects the diverging beam at the back interface of the substrate. The performance of our aSIL setup can in any case be further improved by a careful choice of the lens curvature to optimize the matching with the incoming THz beam and by providing the Si lenses with a broadband anti-reflection coating to further enhance the SNR ²⁹.

To-date, single meta-atom spectroscopy has been possible only with near-field techniques ^{10, 11, 22}. Here we employ the back-to-back aSIL setup to study a single complementary resonator. We previously demonstrated the efficiency of the complementary THz metasurfaces in the context of Landau polaritons³⁰. The significant advantage of this configuration in the transmission measurement of a single resonator is that the measured signal above the noise level is directly the signal of interest yielding a very high contrast. In the case of a standard or direct metasurface (highly transmissive sample), the challenge of the measurement is to detect a very small absorption change on top of a large signal. If one employs a complementary metasurface, the situation is reversed as the transmitted signal is very low, but the only signal detected is the relevant one. Fig. 2 visualizes the reasons that single resonator spectroscopy is possible using an aSIL configuration. The front and back hyperhemispherical Si lenses with a refractive index of $n_r = 3.42$ at $300GHz$ ³¹ focuses the beam onto the resonator plane. The front lens enhances the intensity of the beam arriving at the resonator plane (Fig. 2a) and both lenses expand the accessible wave vectors for far-field propagation (Fig. 2c). The back lens improves the collection of the signal and increases the frequency resolution due to impedance matching and suppression of the echos from the interface

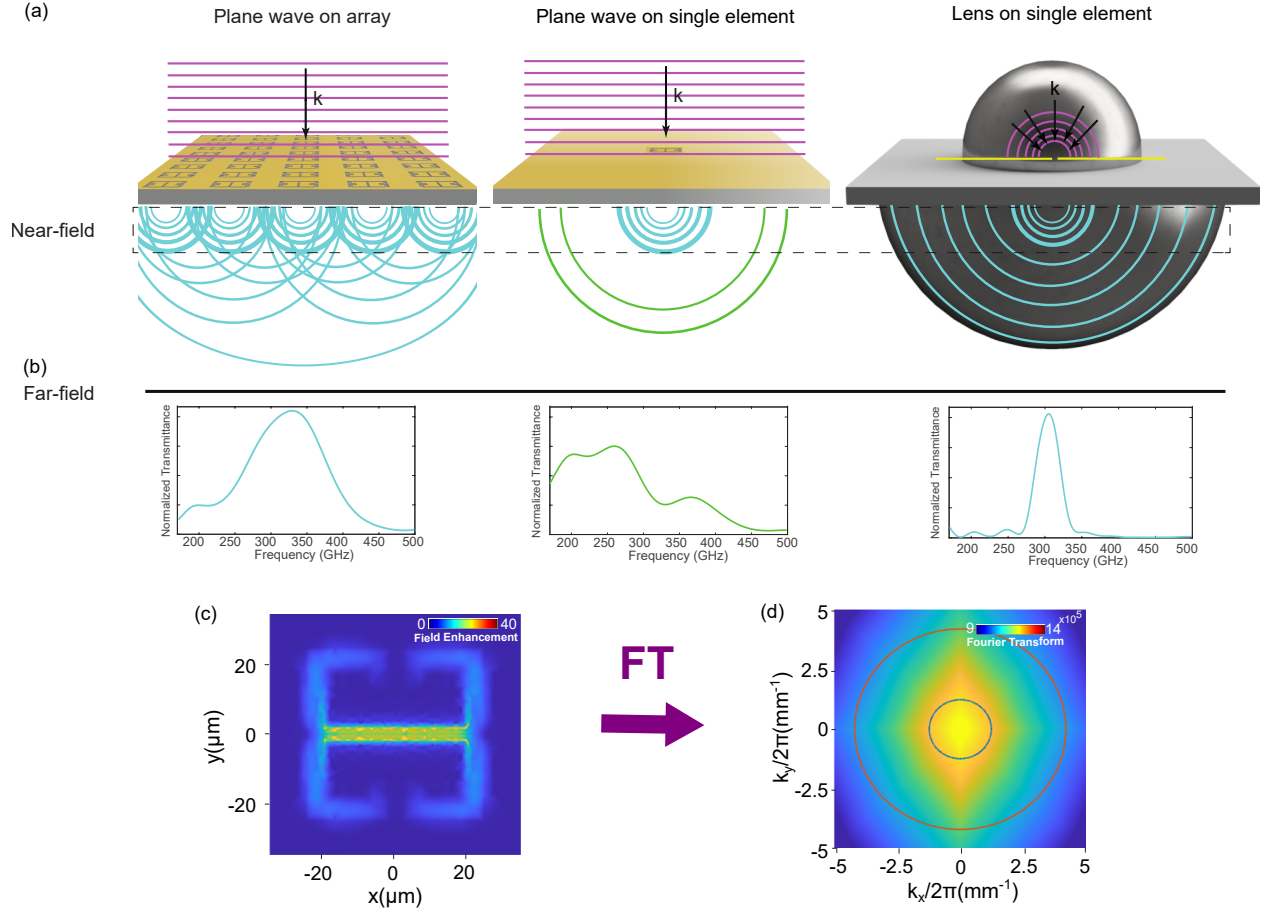


Figure 2: No lens vs. aSIL configuration for Single resonator spectroscopy(a), (b): A schematic of the near-field (a) and far-field (b) of an array without lenses and a single resonator in case of without and with aSIL configuration. (c) The finite element simulation result of the field enhancement at the resonator plane for a single resonator with an incident plane wave with a polarization along y-axis. (d) 2D Fourier transform of the field in panel (c). The blue and red circles represent the accessible wave vectors for far-field propagation in case of having incident waves in the air (without lenses) and in Si(with the aSIL arrangement), respectively.

between back of the sample and the back lens.

In Fig.2 we clarify, using a Fourier optics argument, the mechanism at the basis of the different signals observed when probing a metasurface with a large number of resonator and a single meta-atom with a plane wave compared to the case of a single meta-atom illuminated with an immersion lens. The meta-atoms constituting the planar metamaterial are strongly subwavelength by design: they can be usually probed by far-field optics because the near-field components diffracted by each element are scattered in the far-field by the surrounding elements of the array. The unit cell dimension d_{unit} is highly subwavelength as well (in our case $d_{unit} = 70 \mu\text{m}$ for a free space wavelength $\lambda_{fs} \simeq 1 \text{ mm}$, with $\frac{d_{unit}}{\lambda_{fs}} = 7 \times 10^{-2}$) allowing the spatial frequencies to propagate (Fig. 2a and 2b). The presence of the resonator array is as well required for the excitation of the resonant mode as the nearby elements diffract the incoming wave providing some in-plane components of the wave vectors. In the case where the plane wave illuminates a single subwavelength meta-atom (Fig. 2c) a large portion of spatial frequencies remain trapped in the resonator's near field and do not reach the far-field detector. The corresponding spectrum does not show the resonant feature at 300 GHz. When the aSIL arrangement is used (Fig. 2d), the spread in the wave vector excites the correct resonator mode that can be then collected from the back lens and recover the searched transmission resonance. In the lower row of the figure we plot the near-field electric field distribution and its spatial Fourier transform. The circles correspond to the wave vectors propagating in the case of without lenses (blue) and with lenses (red). It is evident that the quasi totality of wave vectors can propagate in the far-field. As a further confirmation of our model, we can cite the results obtained with a near-field probe measuring a similar complementary single resonator²².

In that experiment, the single resonator was excited with a focusing lens, providing the necessary in-plane k 's. The resonant signal was found to remain trapped in the near field since there was no collecting lens. Now that we clarified the mechanism that underlies the observed transmission spectra, we can discuss the experimental measurements in detail.

As a first step, we perform a systematic study of the cold cavity, illuminating a series of samples deposited onto a semi-insulating GaAs substrate. These samples contain a decreasing amount of resonators, from 3600 down to a single one. We study the linewidth and the transmission amplitude of the cold cavity and their dependency on the number of resonators. The theory of the superradiance^{18,32–34} predicts a reduction in the collective radiative decay and consequently an improvement in quality factor by reducing the number of two-level emitters confined in a spatial region comparable or smaller than the wavelength. This has also been investigated experimentally on metamaterials but never in the single resonator limit³⁵. In order to study this effect, we designed and fabricated 2D array of $n \times n$ complementary split-ring resonators (cSRR), including a very large array of 60×60 resonators and small arrays with a varying n from 6 to 1, operating at a resonant frequency of 350 GHz and a periodicity of $70 \mu m$ on a GaAs substrate (Fig. 1b).

We measured the resonators with a commercial THz spectrometer (details in Methods section) at room temperature. We conducted the measurements with and without the back-to-back aSIL system. As expected²², the resonant peak of 2×2 cSRR array and the single resonator could not be resolved without the use of our aSIL arrangement because of the weak interaction of a few resonator with the THz beam (see the supplementary info). Even the measurement with 9 res-

onators shows a very weak resonant peak. In Fig. 3, we report the result of the study, showing the collected spectra using the aSIL assembly and the extracted quality factors (Q-factor) for measurement with lenses. The measurement shows about 5 times signal enhancement in the time domain for the single resonator. Moreover, the resonant peak for the arrays with less than 9 resonators were resolved with a large dynamic range ($60dB$ for the single resonator).

Another key feature of this technique is the significant improvement in frequency resolution. Since Si and GaAs have very close refractive indexes up to $1THz$ ³¹, the echoes of the THz pulse, reflected at each interface are greatly suppressed due to the impedance matching and, as a consequence, the etalon effects are minimized. Particular care was taken to assemble the stack lens-sample-lens without any air gap, pressing on the assembly with metallic positioners (see Supplementary material). In the best conditions, the resolution was $18GHz$ (corresponding to a time scan length of $55ps$), limited by the reflection from the detector. If we compare the results of the measurements on the large arrays with and without the lenses we observe a difference in the resonant frequency due to the presence of the front Si lens. The presence of an high index material in the near field of the complementary resonators red-shifts the resonance to values below $300GHz$ which is also confirmed by our finite element simulations (more information in the supplementary document).

To calculate the Q factor, we fitted the resonant peak with a Breit-Wigner-Fano (BWF) function. Fig.3 shows an almost constant Q-factor for 3600 to 16 resonators measured with lenses. For the samples with a fewer number of resonators ($n \leq 3$), as the dimension of the resonator

field becomes comparable to the wavelength (at $300GHz$, the wavelength propagating in GaAs, $\lambda_n = \lambda/n_{GaAs} = 278\mu m$ and the one propagating in Si $\lambda_n = \lambda/n_{Si} = 292\mu m$), the quenching of superradiance emerges. The Q-factor doubles from 9 resonators to a single resonator due to the quenching of the superradiant decay and reaches ~ 11 for the single one. This can have important consequences in the context of the strong coupling experiments that we will discuss in the next section. If we compare our results with similar studies performed on arrays of metamaterials down to a few elements ³⁶, we observe a similar behaviour as in the case of "incoherent" resonators that are not coupled by magnetic interaction, since the symmetric arrangement of the inductors in our case cancels out the magnetic response. What is clear in our data is the enhancement of the Q factor when the occupied area by the resonators is smaller than λ^2 . It is worth noting that the number of illuminated resonators in case of the large array (60×60 resonator) are 2628 for the measurement without lenses (a $4mm$ diameter illuminating spot) and 44 for the measurement with aSIL configuration (a $500\mu m$ diameter illuminating spot).

Ultrastrong coupling in a single complementary resonator After having characterized the measurement technique and studied the Q-factor dependence of the cSRR array on the number of resonators, we apply the developed method to the spectroscopy of a single resonator ultrastrongly coupled to an inter-Landau level (LL) transitions in a single GaAs QW. With a similar fabrication process, a large array and a single cSRR were deposited on top of a two dimensional electron gas (2DEG) produced in a single GaAs square QW located $90nm$ below the surface. The sample transmission is then measured in a THz-TDS setup at cryogenic temperature ($T = 2.7K$) as a function of magnetic field swept between 0 and $4T$. The best resolution for this setup is $33GHz$

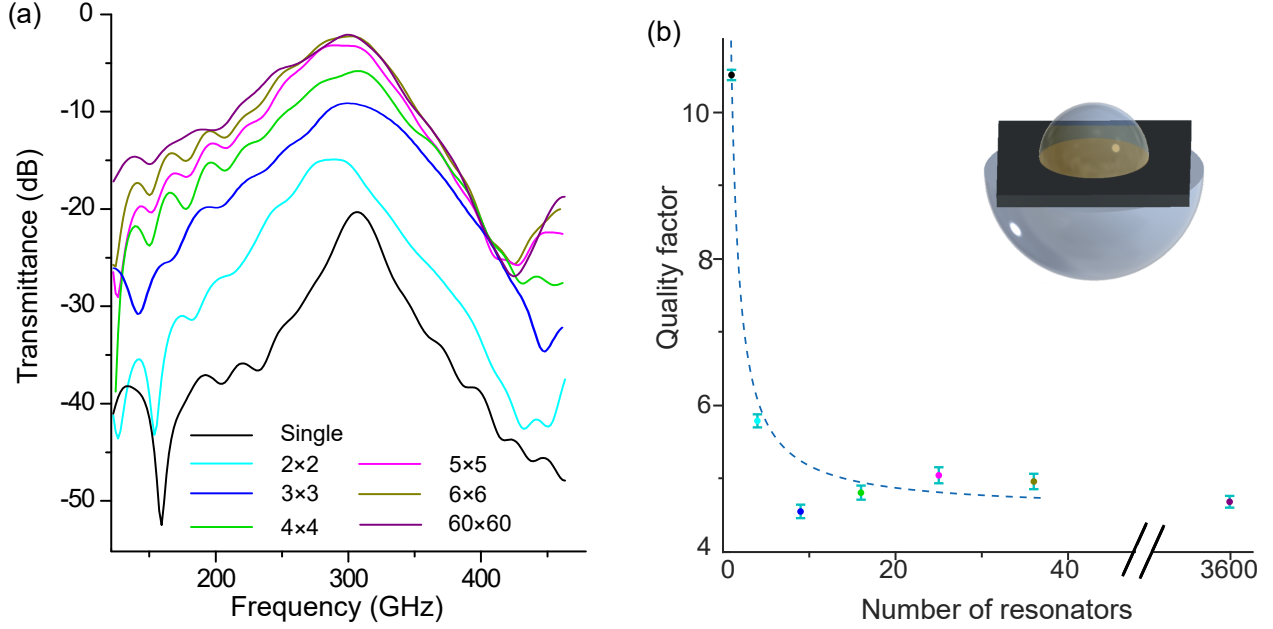


Figure 3: **Quenching of the superradiance decay** (a) Transmittance of $n \times n$ array of cSRRs ($n = 1$ to 6) and a large array with $n = 60$. These measurements are done using the aSIL assembly and the resonant peak of the single resonator is resolved. (b) is Q factor vs. the number of resonators extracted from the measurements with lenses. The color of the data points are the same as the color of the transmittance curves in panel (a). The blue dashed line shows the linear dependence of the quality factor on the density of the resonators ($Q = \frac{6.04}{N} + 4.6$). The Q-factors are calculated using fitting the resonant peak with BWF function. All error bars represent one σ confidence interval.

(corresponding to a time scan length of $30ps$), limited by the thickness of the cryostat windows. Further details are to be found in the Methods section. In order to gain insight into the coupling of the complete metasurface and the single resonator to the THz beam, we measured the transmission spectra for both kind of samples with and without the aSIL assembly. The results, displayed

as transmittance color maps as a function of the magnetic field, are reported in Fig. 4. The figure shows a comparison between the transmission measurements without (top row) and with aSIL configuration (bottom row) for a 2D array of 60×60 resonators (left column) and a single resonator (right column). The colormaps relative to the plane wave (without lenses) case clearly show very well resolved polaritonic branches for the 3600 resonator sample and a very different spectrum in the case of a single resonator. In the single resonator measurement, we observe a broad spectral feature corresponding to high transmission that extends from $180GHz$ to $300GHz$ and is independent from the applied magnetic field. A narrow absorption feature linearly changing with the magnetic field corresponding to the cyclotron resonance is crossing the broad transmission peak. The single resonator excited by a plane wave, whose radiation is collected without an immersion lens, is not showing ultrastrong coupling since the correct resonant LC mode cannot be excited and detected. The measurement in the case of the single resonator measured with the aSIL assembly is significantly different: we observe extremely well resolved polaritonic branches that compare well with the one observed in the 3600 resonator sample in both cases with and without the lenses. We can now analyze in detail and compare the polaritons measured in the case of employing the aSIL assembly for the single resonator and the large array.

The lower polariton (LP) mode of the coupled single resonator at its asymptotic limit, at $B = 4T$, has a Q-factor of 15.4 (using time trace decay method). The Q-factor of the LP at $B = 4T$ for the sample with the coupled 2D array of 3600 resonator without lenses and with lenses are 3.4 and 6.9, respectively. Similar to the cold cavity in the previous section, the Q-factor of the LP at its asymptotic limit is higher for the single resonator compared to the one for the array

due to the quenching of the superradiance decay. By extracting the maximum of the spectrum at each magnetic field and fitting them with Hopfield model⁵, a normalized coupling of $\frac{\Omega}{\omega} = 33\%$ is achieved for the single resonator measured in a confocal configuration. For the array of 3600 resonators the normalized coupling for the measurement with and without lenses are $\frac{\Omega}{\omega} = 32\%$ and 36% , respectively. The cross sections of the colormap of the 60×60 array and the single resonator measurement with lenses at three different magnetic field values of $0T$, $800mT$, and $4T$ show the well resolved upper polariton (UP) and LP peaks in the single resonator measurement (Fig. 4b). We notice that, as expected, the polaritonic branches in the single resonator case display a higher quality factor with respect to the 60×60 array. It is also evident that there is a renormalization of the loaded cavity frequency that blueshifts the resonance by 30 GHz ($\simeq 0.1\omega$) when we reduce the number of resonators from 3600 to 1. Interestingly, the normalized coupling strength remains basically the same ($\frac{\Omega}{\omega}|_{single} = 0.33$, $\frac{\Omega}{\omega}|_{3600} = 0.32$). We do not observe such a shift when we investigate the cold cavity at 300 K (see Fig.3(a)). We attribute this shift to the large dielectric contribution of the 2DEG that effectively produces a slow light effect enhancing the collective Lamb shift of the ensemble of meta atoms as observed in other systems^{37–39}.

The calculated cooperativity for the coupled single resonator measurement is equal to $C = 94$ and for the large array of resonators are $C = 26.4$ without lenses and $C = 37$ with the aSIL configuration.

The cooperativity is calculated using $C = \frac{4g^2}{\kappa\gamma}$ where g is half of the mode splitting at the anti-crossing, κ is the mode dissipation (cavity decay) rate and γ is the decoherence rate. γ is

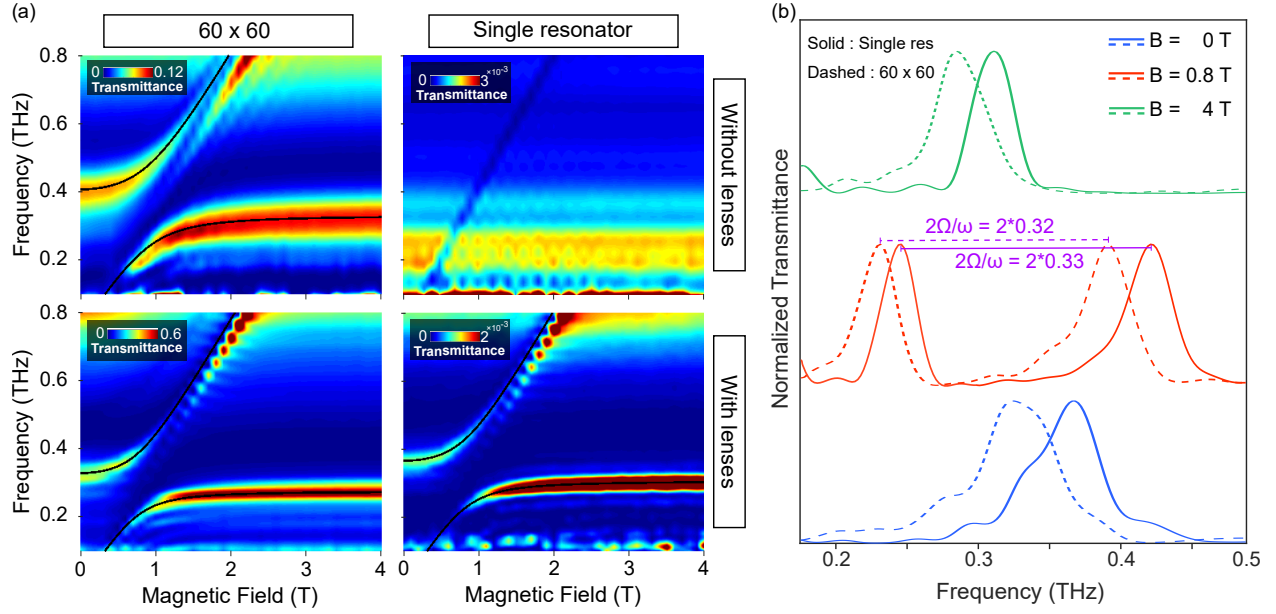


Figure 4: Comparison of THz-TDS measurements of a large array and a single cSRR coupled to LL transitions in a GaAs QW with/without Si lenses(a) The transmission measurements without (top row) and with the aSIL configuration (bottom row) for a 2D array of 60×60 cSRRs (left column) and a single resonator (right column). The polariton branches in the measurement of the single resonator without lenses are not resolved due to the weak interaction of the resonator with the THz beam. The black solid lines are the fitted LP and UP using the Hopfield model. (b) Sections of the colormap for the single resonator (solid lines) and 60×60 array (dashed lines) both measured with lenses at different magnetic field values ($B = 0, 0.8T$, (anti-crossing) and $4T$) to demonstrate the well-resolved polariton branches. The distance between peaks at $B = 0.8T$ which is twice of the vacuum Rabi splitting is marked with purple. All the modes are normalized to their maximum value. The vertical shift is for clarity.

extracted from the direct measurement of the cyclotron coherence time⁴⁰ using TDS measurement of the 2DEG measured with the confocal system. The linewidth of the cyclotron resonance is smaller than the one measured without lenses due to the superradiance effect (more information in the supplementary document). An estimate of the number of optically active electrons at the top most LL for our single cavity with a cavity surface of $S = 155\mu m^2$ on a single GaAs QW yields $n = \frac{eB}{h} \times S = 2.42 \times 10^{14} [\frac{1}{m^2 T}] \times B \times S \simeq 30000$ (Ref²⁰).

In order to increase the coupling and reduce the number of optically active electrons, we employ an Indium Antimonide (InSb)-based 2DEG^{41,42} at the same distance from the surface as the GaAs 2DEG (90 nm). Due to the lighter effective mass of electrons in InSb ($m_{eff} = 0.0225m_0$), the anti-crossing for the coupled system lies at a much lower magnetic field value (250mT compared to GaAs at 800mT) for the same resonator frequency of 300GHz (Fig. 5a). Therefore, the number of coupled electrons is reduced more than 3 times with respect to the GaAs case. To further reduce the cavity volume and increase the field confinement, a single cSRR with a narrower gap of $1\mu m$ at the same resonant frequency (300GHz) is also fabricated and measured (Fig. 5b). To enhance the coupling, this cavity is deposited onto a shallower InSb 2DEG with the same QW thickness at a distance of 50nm below the surface. The cavity surface, evaluated with finite element simulations, is $S = 138.32\mu m^2$ for the larger gap and $S = 28.8\mu m^2$ for the smaller gap. The number of coupled electrons at the anti-crossing are then $n_e = 8368$ and $n_e = 2090$ ²⁰ for the resonators with the gap size of $4\mu m$ and $1\mu m$, respectively.

If we extrapolate this result and consider the case of our previously demonstrated highly

confined, hybrid dipole antenna split-ring resonator²⁰ the use of an InSb QW can lead to an ultra-strongly coupled system with less than 5 coupled electrons.

Due to a higher absorption in InSb QWs, the transmitted signal is less than in the single resonator measurement on GaAs-based QW. The LP mode at its asymptotic limit (at $B = 4T$) has a Q-factor of 6.4 in both cases. The normalized coupling strengths are increased and equal to $\frac{\Omega}{\omega} = 47\%$ and 60% for a single cSRR with $4\ \mu m$ and $1\ \mu m$ gap (more information about the fitting in the supplementary document). The cooperativity in the case of these InSb based samples are $C_{gapsize:4\mu m} = 12.5$ and $C_{gapsize:1\mu m} = 14$. The lower cooperativity (compared to the values for a single resonator on a single GaAs QW) despite having a higher coupling strength is due to an order of magnitude lower mobility in InSb QWs which affects the decoherence rate (larger γ).

The cross sections of the colormaps of the single resonator on InSb QWs measured with lenses at three different magnetic field values of $0T$, $425mT$, and $1.5T$ show the well resolved upper polariton (UP) and LP peaks in the single resonator measurement (Fig. 4c , 4d). Since UP and LP are not both visible at the anti-crossing ($\sim 250 - 300mT$), a cross section at a slightly higher value at $B = 425mT$ is represented. It is worth noting that in the narrower gap resonator, the broadening of UP and partially disappearance of LP at low values of the magnetic field are ascribed to their coupling to a continuum of magnetoplasmon excitations as recently discussed in Ref⁴³.

To conclude, we presented a back-to-back Si immersion lens setup with an asymmetric configuration allowing the spectroscopy of highly subwavelength individual THz cavities. Using this platform, we resolved the far-field transmission measurements of an ultrastrongly coupled, sub-

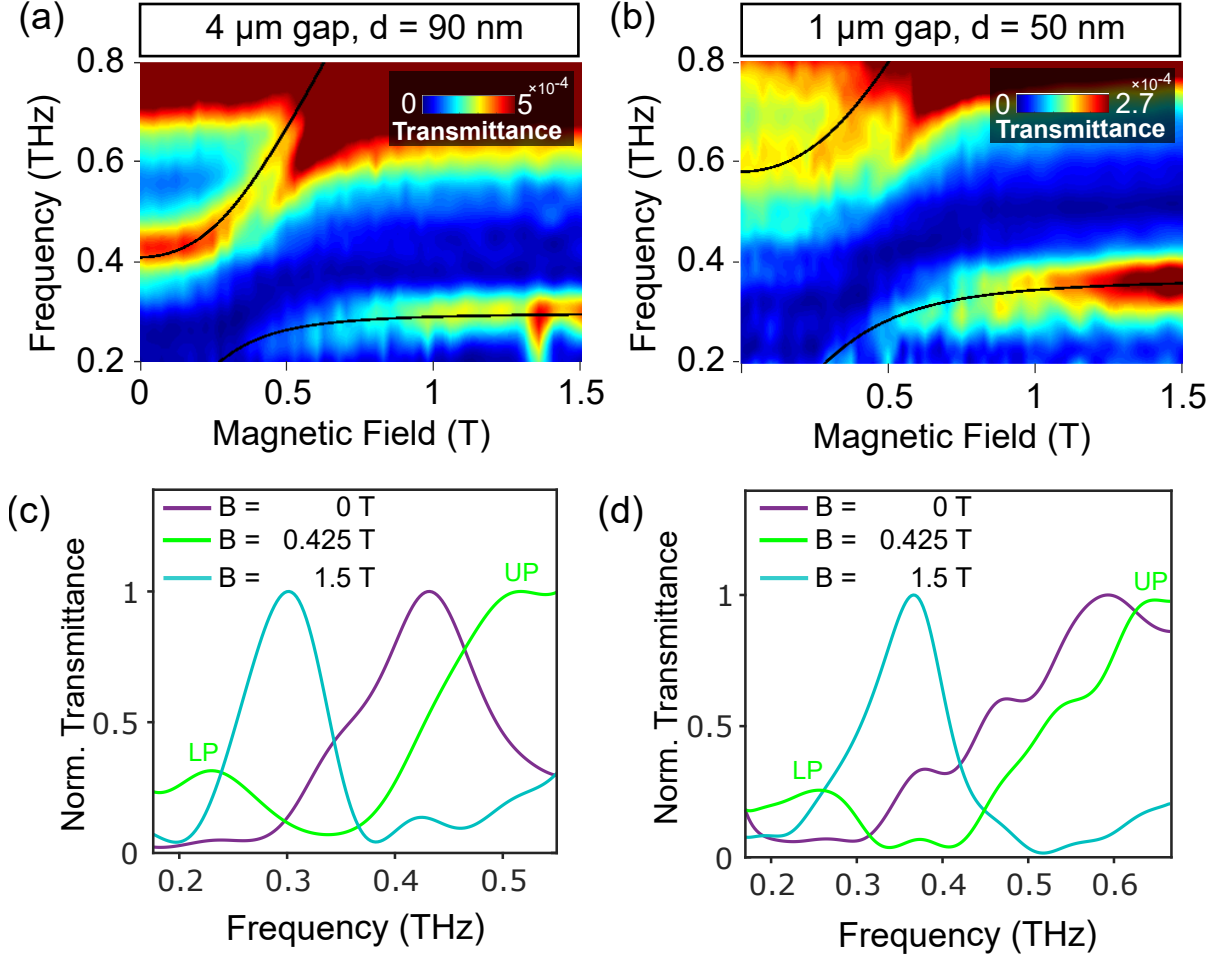


Figure 5: **THz-TDS measurements of LL transitions in a single InSb QW coupled to a single resonator** (a) and (b): The colormaps correspond to the resonators with a gap size of 4 μm on a InSb QW located at a distance of 90 nm below the surface (a) and a gap size of 1 μm on a shallower InSb QW located at a distance of 50 nm below the surface (b), measured with lenses. They show normalized coupling ratio of $\frac{\Omega}{\omega} = 47\%$ and 60% and cooperativity of $C = 12.5$ and 14 , respectively. The black solid lines are the fitted LP and UP using the Hopfield model. (c) and (d): Sections of the colormaps in panel (a) and (b) are represented in panel (c) and (d), respectively, at different magnetic field values ($B = 0, 0.425\text{T}$ and 1.5T). To have a more visible LP and UP, a section at $B = 0.425\text{T}$ which is at a marginally higher value than the anti-crossing is chosen.

wavelength split-ring single resonator to a LL transition in a single GaAs QW and a single InSb QW. The highest coupling of 60% for only about 2000 coupled electrons is reported for a single cSRR on a single InSb QW. As our results demonstrate, the combination of the aSIL configuration with a complementary-based resonant metallic structure paves the way to single-object, highly subwavelength spectroscopy of quantum electrodynamics systems operating in the mm-wave and THz range. The proposed experimental scheme can be extended to the study of dynamical optical conductivity of high-quality 2D structures (graphene, TMDc's, Van der Waals heterostructures)⁴⁴ with very small effective areas (i.e. $10 \times 10 \mu\text{m}^2$) resulting from exfoliation procedures.

Methods

Asymmetric lens setup and sample fabrication The lenses are hyperhemispherical and hemispherical ones fabricated with high resistivity Silicon (Tydex⁴⁵) of diameter $2r_1 = 4\text{mm}$ and $2r_2 = 8\text{mm}$, respectively. The complementary sample layout is conceived in order to ease the alignment of the front lens. The sample is metallized with a circular boundary with a diameter of 4mm , matching the edge of the top lens (see Fig.1c). The lens and the sample can be then accurately aligned under the optical microscope. Mechanical clamps ensure a close contact of the whole assembly front lens-sample-back lens, forming a quasi-index matched ($n_{Si}^{350\text{GHz}} = 3.42$, $n_{GaAs}^{350\text{GHz}} = 3.52$) stack of total length $L_s \simeq 6.5\text{mm}$. The resonators were simulated using a commercial software package (CST microwave studio) and fabricated with a direct laser writing lithography with Heidelberg DWL66+ followed by deposition of 5nm Titanium and 200nm of gold and a lift-off process.

THz-TDS spectrometer The measurements of the Q-factor of the cold cavity as a function of the number of resonators have been carried out with a commercial, fiber coupled THz-TDS spectrometer (Menlo Terasmart⁴⁶). THz radiation is produced and detected by a pair of InGaAs-based photoconductive antennas. The beam is guided with TPX lenses with focal length of 50mm . The whole optical path is contained in a nitrogen purged box. The measurements with the applied magnetic field are performed with a home-made THz-TDS system based on a Ti:Sapphire ultrafast ($\tau < 100$ fs) laser (Mai Tai, Spectra Physics⁴⁷) that illuminates (600mW avg power) an interdigitated photoconductive antenna²⁷. The THz beam is coupled to a Spectromag cryostat (Oxford Instruments⁴⁸) equipped with an 11T superconducting magnet and crystalline quartz (z-cut) windows. Two mirrors (197mm focal length, $2''$ diameter) focus the THz signal at the center of the superconducting coils. A variable temperature insert is used to cool down the sample at $T = 3\text{K}$. The THz signal is then detected via electro-optic sampling in a 3mm ZnTe crystal.

Data Availability Statement The numerical simulation and measurement data that support the plots within this paper are available from the corresponding author upon reasonable request.

1. Chikkaraddy, R. *et al.* Single-molecule strong coupling at room temperature in plasmonic nanocavities. *Nature* **535**, 127 (2016).
2. Iga, K. Surface-emitting laser - Its birth and generation of new optoelectronics field. *IEEE JOURNAL OF SELECTED TOPICS IN QUANTUM ELECTRONICS* **6**, 1201–1215 (2000).
3. Schuller, J. A. *et al.* Plasmonics for extreme light concentration and manipulation. *NATURE MATERIALS* **9**, 193–204 (2010).
4. Kavokin, A., Baumberg, J., Malpuech, G. & Laussy, F. Microcavities, 2nd Edition. In *MICROCAVITIES, 2ND EDITION*, vol. 21 of *Series on Semiconductor Science and Technology*, 1–592 (2017).
5. Hagenmüller, D., De Liberato, S. & Ciuti, C. Ultrastrong coupling between a cavity resonator and the cyclotron transition of a two-dimensional electron gas in the case of an integer filling factor. *Phys. Rev. B* **81**, 235303 (2010).
6. Ballarini, D. & De Liberato, S. Polaritonics: from microcavities to sub-wavelength confinement. *NANOPHOTONICS* **8**, 641–654 (2019).
7. Forn-Díaz, P., Lamata, L., Rico, E., Kono, J. & Solano, E. Ultrastrong coupling regimes of light-matter interaction. *Rev. Mod. Phys.* **91**, 025005 (2019).

8. Malerba, M. *et al.* Towards strong light-matter coupling at the single-resonator level with sub-wavelength mid-infrared nano-antennas. *Applied Physics Letters* **109** (2016).
9. Todorov, Y. *et al.* Ultrastrong light-matter coupling regime with polariton dots. *Phys. Rev. Lett.* **105**, 196402 (2010).
10. Gillibert, R. *et al.* Nanospectroscopy of a single patch antenna strongly coupled to a mid-infrared intersubband transition in a quantum well. *Applied Physics Letters* **117**, 101104 (2020).
11. Wang, C.-F. *et al.* Observation of intersubband polaritons in a single nanoantenna using nano-fir spectroscopy. *Nano Letters* **19**, 4620–4626 (2019).
12. Scalari, G. *et al.* Ultrastrong coupling of the cyclotron transition of a 2d electron gas to a thz metamaterial. *Science* **335**, 1323–1326 (2012). arXiv:<https://science.sciencemag.org/content/335/6074/1323.full.pdf>.
13. Mornhinweg, J. *et al.* Tailored subcycle nonlinearities of ultrastrong light-matter coupling. *Phys. Rev. Lett.* **126**, 177404 (2021).
14. Zhang, Q. *et al.* Collective non-perturbative coupling of 2D electrons with high-quality-factor terahertz cavity photons. *NATURE PHYSICS* **12**, 1005+ (2016).
15. Paravicini-Bagliani, G. L. *et al.* Magneto-transport controlled by Landau polariton states. *NATURE PHYSICS* **15**, 186+ (2019).

16. Appugliese, F. *et al.* Breakdown of the topological protection by cavity vacuum fields in the integer quantum hall effect. *ARXIV 2107.14145* (2021).
17. Bayer, A. *et al.* Terahertz light-matter interaction beyond unity coupling strength. *Nano Letters* **17**, 6340–6344 (2017).
18. Dicke, R. H. Coherence in spontaneous radiation processes. *Phys. Rev.* **93**, 99–110 (1954).
19. Todorov, Y. & Sirtori, C. Few-electron ultrastrong light-matter coupling in a quantum *LC* circuit. *Phys. Rev. X* **4**, 041031 (2014).
20. Keller, J. *et al.* Few-electron ultrastrong light-matter coupling at 300 ghz with nanogap hybrid lc microcavities. *Nano Letters* **17**, 7410–7415 (2017).
21. Jeannin, M. *et al.* Absorption Engineering in an Ultrasubwavelength Quantum System. *NANO LETTERS* **20**, 4430–4436 (2020).
22. Hale, L. L. *et al.* Noninvasive Near-Field Spectroscopy of Single Subwavelength Complementary Resonators. *LASER & PHOTONICS REVIEWS* **14** (2020).
23. Zumofen, G., Mojarad, N. M., Sandoghdar, V. & Agio, M. Perfect reflection of light by an oscillating dipole. *Phys. Rev. Lett.* **101**, 180404 (2008).
24. Sondermann, M. *et al.* Design of a mode converter for efficient light-atom coupling in free space. *APPLIED PHYSICS B-LASERS AND OPTICS* **89**, 489–492 (2007). Spring Meeting of the Quantum Optics and Photonics Section of the German-Physical Society, Dusseldorf, GERMANY, 2007.

25. Pinotsi, D. & Imamoglu, A. Single photon absorption by a single quantum emitter. *Phys. Rev. Lett.* **100**, 093603 (2008).
26. Vamivakas, A. N. *et al.* Strong extinction of a far-field laser beam by a single quantum dot. *Nano Letters* **7**, 2892–2896 (2007). PMID: 17691853, arXiv:<https://doi.org/10.1021/nl0717255>.
27. Madeo, J. *et al.* Frequency tunable terahertz interdigitated photoconductive antennas. *ELECTRONICS LETTERS* **46**, 611–U25 (2010).
28. Gallot, G. & Grischkowsky, D. Electro-optic detection of terahertz radiation. *J. Opt. Soc. Am. B* **16**, 1204–1212 (1999).
29. Gan, Y. *et al.* 3.9 thz spatial filter based on a back-to-back si-lens system. *Opt. Express* **28**, 32693–32708 (2020).
30. Maissen, C. *et al.* Ultrastrong coupling in the near field of complementary split-ring resonators. *Phys. Rev. B* **90**, 205309 (2014).
31. Grischkowsky, D., Keiding, S., van Exter, M. & Fattinger, C. Far-infrared time-domain spectroscopy with terahertz beams of dielectrics and semiconductors. *J. Opt. Soc. Am. B* **7**, 2006–2015 (1990).
32. Keller, J. *et al.* Superradiantly limited linewidth in complementary thz metamaterials on si-membranes. *Advanced Optical Materials* **6**, 1800210 (2018). arXiv:<https://onlinelibrary.wiley.com/doi/pdf/10.1002/adom.201800210>.

33. Sersic, I., Frimmer, M., Verhagen, E. & Koenderink, A. F. Electric and magnetic dipole coupling in near-infrared split-ring metamaterial arrays. *Phys. Rev. Lett.* **103**, 213902 (2009).
34. Jenkins, S. D. & Ruostekoski, J. Resonance linewidth and inhomogeneous broadening in a metamaterial array. *Phys. Rev. B* **86**, 205128 (2012).
35. Choudhary, S. *et al.* Weak superradiance in arrays of plasmonic nanoantennas. *Phys. Rev. A* **100**, 043814 (2019).
36. Fedotov, V. A. *et al.* Spectral collapse in ensembles of metamolecules. *Phys. Rev. Lett.* **104**, 223901 (2010).
37. Yao, P. *et al.* Ultrahigh purcell factors and lamb shifts in slow-light metamaterial waveguides. *Phys. Rev. B* **80**, 195106 (2009).
38. Frucci, G. *et al.* Cooperative lamb shift and superradiance in an optoelectronic device. *New Journal of Physics* **19**, 043006 (2017).
39. Wen, P. Y. *et al.* Large collective lamb shift of two distant superconducting artificial atoms. *Phys. Rev. Lett.* **123**, 233602 (2019).
40. Wang, X., Hilton, D. J., Reno, J. L., Mittleman, D. M. & Kono, J. Direct measurement of cyclotron coherence times of high-mobility two-dimensional electron gases. *Opt. Express* **18**, 12354–12361 (2010).
41. Keller, J. *et al.* Landau polaritons in highly nonparabolic two-dimensional gases in the ultra-strong coupling regime. *Phys. Rev. B* **101**, 075301 (2020).

42. Lehner, C. A. *et al.* Limiting scattering processes in high-mobility insb quantum wells grown on gasb buffer systems. *Phys. Rev. Materials* **2**, 054601 (2018).
43. Rajabali, S. *et al.* Polaritonic nonlocality in light–matter interaction. *Nature Photonics* **15**, 690–695 (2021).
44. Ajayan, P., Kim, P. & Banerjee, K. Two-dimensional van der waals materials. *Physics Today* **69**, 38–44 (2016). arXiv:<https://doi.org/10.1063/PT.3.3297>.
45. Tydex. http://www.tydexoptics.com/products/thz_optics/thz_lens/.
46. Menlo Systems GmbH. <https://www.menlosystems.com/products/thz-time-domain-solutions/terasmart-terahertz-spectrometer/>.
47. Spectra Physics
. <https://www.spectra-physics.com/f/mai-tai-ultrafast-laser>.
48. Oxford Instruments NanoScience
. <https://nanoscience.oxinst.com/products/spectromagpt>.

Acknowledgements G.S. would like to thank R. Singh and F. Helmrich for discussions. We acknowledge financial support from ERC Grant No. 340975-MUSiC and the Swiss National Science Foundation (SNF) through the National Centre of Competence in Research Quantum Science and Technology (NCCR QSIT).

Competing Interests The authors declare that they have no competing financial interests.

Authors contributions G. S. and S.M. conceived the aSIL configuration. S.R. fabricated the samples. S.R. and E.J. performed the measurements. M.B., C.L. and W.W. performed the epitaxial growth. Data interpretation and discussion was made by J.F., G.S., S.R, E. J. and S.M. G.S. and S.R. wrote the manuscript. All the work was made under the supervision of J.F. and G.S.

Correspondence *Correspondence should be addressed to S. Rajabali (email: shimar@phys.ethz.ch) and G. Scalari (email: scalari@phys.ethz.ch).